Fractionation of Suspensions Using Synchronized Ultrasonic and Flow Fields

Zenon I. Mandralis and Donald L. Feke
Dept. of Chemical Engineering, Case Western Reserve University, Cleveland, OH 44106

A fractionation method for fine-particle suspensions using resonant ultrasonic fields coordinated with bidirectional fluid flow fields is described. The basis for the separation is differences in the speed of response of particles to the imposition of a resonant acoustic field. As such, the method is sensitive to the particle size and the acoustic contrast between the solid particles and their suspending fluid. Both batch and continuous fractionation processes can be developed from a two-step acoustic-flow cycle. An analytical model was constructed from equations that describe the trajectories of particles as they respond to the acoustic and flow fields. Model predictions indicate how the fractionation can be controlled through choice of cycle parameters. The method was implemented experimentally. Results for the fractionation of 325-mesh polystyrene spheres indicate that sharp fractionations can be achieved. The experimental results are generally in agreement with the model predictions.

Introduction

The ability to fractionate dispersions or to manipulate physical characteristics such as the size distribution within fine-particle suspensions can have important applications in many industries. Many separation and reaction processes (extraction from solids, adsorption onto solids, or fluidization of catalysts, for example) could benefit by operating with only small particles. Small particles have large interfacial area per unit volume of solids as well as decreased internal resistances to heat and mass transfer. In other cases, it is useful to have a very narrow particle-size distribution. In the medical sciences, for example, sharply fractionated particles could have many potential applications in diagnosis and treatment. Ceramic particles having narrow size distribution may lead to improved material properties. Also, in chromatographic separations, monodisperse packings lead to better resolution.

During the last decade, there has been a growing interest in the manipulation of particles, droplets or bubbles suspended in liquids or gases by forces associated with resonant acoustic fields. The response of particles subjected to various combinations of acoustic forces with hydrodynamic, gravitational or diffusion forces has been experimentally studied (Higashitani et al., 1981; Mandralis et al., 1990; Mandralis and Feke, 1992; Tolt and Feke, 1991) and modeled (Haar and Wyard, 1978; Weiser and Apfel, 1982; Mandralis et al., 1990; Tolt and Feke, 1988; Collas et al., 1989). Suspended particles respond to resonant fields if there is a nonzero acoustic contrast between the particles and their suspending fluid. The acoustic force that acts on particles is sensitive to the size of the particles as well as the density and compressibility of both the solids and their suspending fluids.

In many of the previously developed separation methods, acoustic forces can be used to drive particles to and hold them at certain positions within the acoustic standing wave field. The ultimate separation is achieved by either removing the fluid while the particles are held fixed (Tolt and Feke, 1992; Schram and Rendell, 1989) or by transporting the particles through the fluid using "drifting" resonant acoustic fields (Tolt and Feke, 1992; Hager et al., 1991; Whitworth et al., 1991; Schram, 1988; Schram and Rendell, 1989; Peterson, 1988). In all of these methods, the principal direction of propagation of the acoustic field coincides with the flow direction. During the harvesting of particles, the acoustic force must exceed the drag forces produced. To increase separation efficiency and the speed of recovery of particles, it is possible to increase the acoustic force through inducing particle agglomeration with secondary acoustic forces. This practice,

Correspondence concerning this article should be addressed to D. L. Feke.

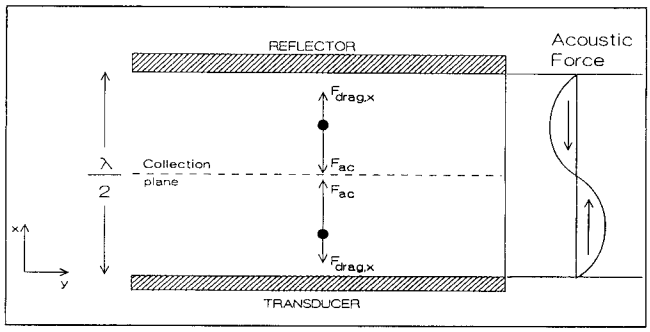

Figure 1. Separation chamber used to illustrate the fractionation principle.

however, would be detrimental to achieving sharp fractionation.

In this article, we report on a new method for fractionating liquid suspensions of fine particles, 0.1–100 μm in size, on the basis of a combination of particle size and acoustic constant. The fractionation occurs in a relatively long and wide rectangular chamber of narrow cross-section and utilizes orthogonal acoustic and flow fields. The process utilizes the transient response of the particles to resonant acoustic fields that are cycled between two different frequencies. Bidirectional, laminar flows along the chamber are coordinated with the cyclic resonant fields to achieve the fractionation.

The next section justifies using the transient response of suspended particles to the acoustic fields as a basis for the separation. Following this, the process concept is described. Next, results from a theoretical model of the process demonstrate the potential effectiveness of the technique. Finally, proof-of-principle experimental results for the continuous fractionation of nominally 325-mesh polystyrene particle suspensions are presented.

Basis for the Separation

Consider a planar acoustic transducer and a parallel reflector as shown in Figure 1. A resonant acoustic field of wavenumber κ is established in the chamber. The spacing between the transducer and reflector is adjusted to accommodate one-half wavelength of sound at this frequency. An initially uniform suspension of fine particles occupies the volume of this chamber.

An order of magnitude analysis shows that the principal forces acting on particles in the chamber are due to primary acoustic, hydrodynamic and gravitational effects. (See the Appendix for a discussion of acoustic forces on suspended particles). For the present, assume that the particles are neutrally buoyant so that gravity can be neglected. If the viscous relaxation time is short, the migration of any particle in response to a resonant acoustic field is determined from:

$$-6\pi\mu R\frac{\partial x}{\partial t}+4\pi R^3\kappa E_{ac}F\sin(2\kappa x)=0 \qquad (1)$$

for the x direction. In Eq. 1 the two terms represent the viscous drag and primary acoustic force acting on the particles.

Ignoring agglomeration, the number of particles within the chamber is constant. Thus, the number density of particles

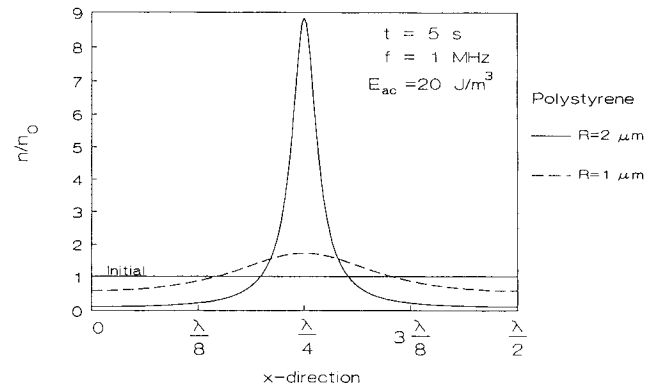

Figure 2. Concentration profiles for 1- and 2-μm polystyrene particles after 5 s of 1 MHz, 20 J/m^3 ultrasound.

Note that the differences in response speed enriches the nodal region with large particles.

averaged over the y direction must be subject to the conservation equation

$$\frac{\partial n}{\partial t}+\frac{\partial}{\partial x}\left(n\frac{\partial x}{\partial t}\right)=0. \qquad (2)$$

For the case of a uniform initial particle distribution of number density n_0, Eqs. 1 and 2 can be solved simultaneously to give the kinetics of particle collection within the standing acoustic field:

$$\frac{n}{n_0}=\frac{\sin\{2\arctan[\exp(4\kappa^2E_{ac}R^2Ft/3\mu)\tan(\kappa x)]\}}{\sin(2\kappa x)} \qquad (3)$$

From Eq. 3 it can be seen that the response of particles to the applied sound field is a function of the frequency and the energy density of the acoustic field as well as the particle size and the acoustic contrast factor.

To illustrate the variation of the transient response of particles with their properties, Figure 2 depicts the concentration profile for polystyrene particles of 1-μm and 2-μm radius after 5 s of irradiation with an 1 MHz, 20 J/m^3 standing wave field. Both types of particles collect at the nodal position ($x=\lambda/4$) but at different rates due to their sizes. At short times after the application of the acoustic field, the nodal region of the acoustic chamber is enriched with larger particles while the antinodal regions are enriched with smaller particles. Ultimately, all particle will be driven to the nodes. However, the partial separation achieved in the cross section at short times can be amplified into a useful separation along the channel by coordinated, bidirectional laminar flows.

Process Concept

Consider the same geometric configuration as depicted in Figure 1, but allow for laminar flow to be generated in the y direction using an external pumping circuit. For flow in the narrow slit, we assume that the viscous relaxation time is short and that the particles do not disturb the flow. Thus, the fluid velocity in the y direction is:

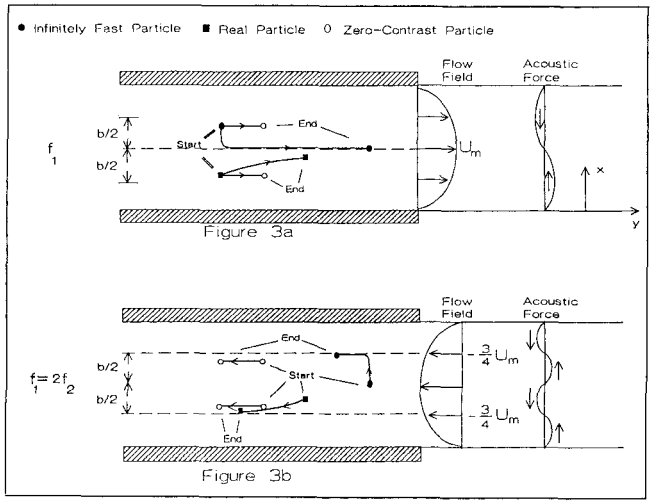

Figure 3. Trajectories of a hypothetical infinitely fast particle and a zero-contrast particle, as well as a real particle, to the acoustic-flow cycle: (a) step 1; (b) step 2.

$$u_f = \frac{3Q}{4b^3} x(2b-x). \tag{4}$$

To illustrate the operation principle, it is possible to follow the trajectories of three hypothetical particles to a combined acoustic and flow cycle. Two of these particles represent limiting cases; an infinitely fast particle (one which instantaneously migrates to a nodal position) and a zero-contrast particle (one that is totally insensitive to acoustic forces and hence can be used to track fluid motion). The third type of particle is a real particle which responds to the acoustic force at a nonzero, but finite rate. This particle represents one particle type in a suspension that may contain a variety of particles having a range of response speeds.

For ease of illustration, the starting positions of the infinite-contrast and real particles are depicted to be symmetric with respect to the midplane of the chamber in Figure 3a. Due to the symmetry of both the acoustic and flow fields, these are equivalent positions. A zero-contrast particle is also depicted to initially coincide with both the real and infinite-contrast particle. Also, the initial x positions of the particles are all located within $b/2$ of the midplane. This is not an arbitrary choice since, as discussed in the next section, after the repeated application of the acoustic cycle, all particles will be located within $b/2$ of the midplane.

In response to an acoustic field of frequency f_1, the infinitely fast particle moves immediately to the node, the real particle moves toward the nodal plane at a finite rate, and the zero-contrast particles maintain their original x positions. Simultaneously, the laminar flow field of the flow rate Q_1 is introduced that transports all particles to the right for a duration t_1. As a consequence of the parabolic shape of the flow profile, the final position of the infinitely fast particle is further to the right than that of the real particle, which in turn is located further to the right than the zero-constant particle. Figure 3a depicts this qualitatively.

Next, suppose the acoustic frequency is doubled ($f_2 = 2f_1$) so that additional collection planes are formed at the two positions midway between the center of the chamber and the walls (Figure 3b). Simultaneously, a leftward laminar flow Q_2 is applied for duration t_2. Figure 3b qualitatively depicts the particle trajectories during this step. If the strength of the acoustic field is high enough so that significant vertical migration of the particles is realized, the parabolic flow profile will transport the infinitely fast particle less leftward than the zero-contrast particle.

Over the course of one cycle, the net displacement of each particle can be calculated assuming that the particles follow the fluid motion in the lateral direction. For convenience, we define the parameter δ as the ratio of flow rates in the two steps,

$$\delta \equiv \frac{Q_2}{Q_1} \tag{5}$$

and α to be the relative volumes of fluids displaced in the two steps of the cycle,

$$\alpha \equiv \frac{Q_2 t_2}{Q_1 t_1} = \delta \frac{t_2}{t_1}. \tag{6}$$

After completion of the two-step cycle, the zero-contrast particles (and the fluid) will experience a net displacement in the y direction of

$$\Delta y_{zc} = \frac{3x(2b-x)}{4b^3} (Q_1 t_1 - Q_2 t_2) = \frac{3x(2b-x)}{4b^3} Q_1 t_1 (1-\alpha) \tag{7a}$$

while the infinitely fast particle is displaced

$$\Delta y_{if} = \frac{3}{4b} \left(Q_1 t_1 - \frac{3}{4} Q_2 t_2\right) = \frac{3}{4b} Q_1 t_1 \left(1 - \frac{3}{4}\alpha\right). \tag{7b}$$

Note that if $1 < \alpha < 4/3$, the two limiting types of particle could be driven in opposite directions over the course of the two-step cycle. The net displacement of real particles will fall between the limits given by Eqs. 7a and 7b. By choosing appropriate operating parameters, the scheme described above can be used to fractionate particles in either a batch or continuous mode as described below.

Batch Fractionation

Suppose the flow parameters were chosen such that $\alpha = 1$. Then, Eq. 7a predicts that there will be no net displacement of a zero-contrast particle (or the fluid) at the completion of one cycle. All real particles will acquire a net displacement to the right. Hence, repetition of the cycle will result in a translation of all particles toward the right end of the chamber but with different effective speeds.

Figure 4 shows an example of the trajectories of two types of real particles, 3- and 10-μm polystyrene spheres ($F = 0.23$) in aqueous suspension. The acoustic energy densities in both steps of the cycle are identical at $E_{ac,1} = E_{ac,2} = 10$ J/m^3, while the flow parameters are $t_1 = t_2 = 4$ s and $Q_1 = Q_2 = 7.36 \times 10^{-6}$ m^2/s. The two acoustic frequencies used are 0.7 and 1.4 MHz.

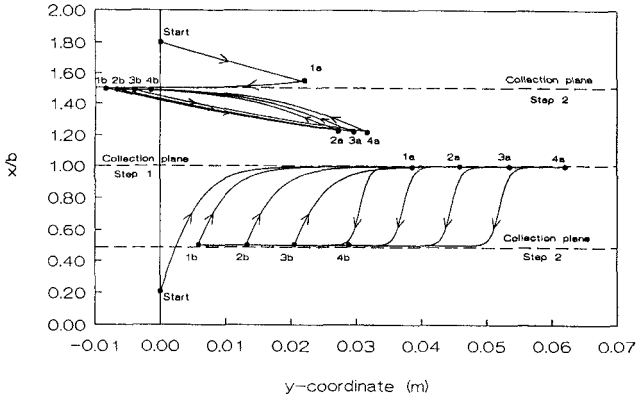

Figure 4. Predicted trajectories of two types of polystyrene particles in response to the acoustic-flow cycle.

The solid points indicate the locations of the particles at the end of each step of four cycles. The labels by the points indicate the cycle number, as well as the step (a = step 1; b = step 2). Note that the particles have different effective translation rates along the chamber.

The initial locations of the particles are at symmetric positions with respect to the midplane, $x/b=0.2$ and $x/b=1.8$. The trajectories during four cycles are depicted. The solid points on the graphs indicate the positions of the particles at the end of each step of the cycle.

Note that there is a differential rate of progression of the two particle types along the chamber (compare positions 1b through 4b for each particle). By sequentially harvesting particles at the right end, a chromatographic fractionation can be achieved. Note also that in this example, the initial positions of the particles were selected to be more than $b/2$ from the midplane of the chamber. After a small number of cycles, the vertical positions of the particles typically approaches a limit cycle located entirely within $b/2$ of the midplane. This results because the acoustic force alternately drives particles toward the midplane of the chamber (during the first step of the cycle) or toward a plane located $b/2$ from a wall (during the second step of the cycle). Since at no time in the cycle is there an acoustic force which drives particles closer than $b/2$ to the wall, these regions will ultimately be stripped of all particles.

Continuous Fractionation

Suppose the method is operated such that $1<\alpha<4/3$. In this case, there is a net displacement of zero-contrast particles (and fluid) to the left ($\Delta y_{zc}<0$) and a net displacement of infinitely fast particles to the right ($\Delta y_{if}>0$) after one cycle. The direction of travel of a real particle would depend on its acoustic response speed. For instance, if the net leftward flow rate of fluid averaged over one cycle is intermediate between the effective migration rates of the two particles exemplified in Figure 4, then the smaller particle would move leftward, while the larger particle would move rightward over the course of one cycle. Correspondingly, for a given starting position, there would be some size of real particles (denoted the cut size) that would experience a zero net displacement during over one cycle.

The net flow rate of product obtained at the left end of the chamber, Q_{prod}, is:

$$Q_{\text{prod}} = Q_1(\alpha-1)\frac{\delta}{\delta+\alpha} \tag{8}$$

To make the process continuous, suspension can be fed into the chamber at the right end at an equivalent rate. Particles faster than the cut particle would be harvested at the right, while fluid containing particles slower than the cut particle would emerge with the fluid product at the left of the chamber. Note that operation with $\alpha>4/3$ does not result in a fractionation since all particle types would be transported to the left end of the chamber. Note also that there is a direct relationship between the operating parameters for the acoustic and flow cycles and the characteristics of the cut particle. Thus, by changing the operating parameters for the acoustic/flow cycle, a single apparatus has flexibility to perform a wide range of fractionations.

The next section describes a model that is used to determine the characteristics of the cut particle when the acoustic and flow field parameters are known.

Process Model

The trajectory of individual particles are given by Eq. 1 for the x direction and by

$$6\pi\mu R\left(u_f-\frac{\partial y}{\partial t}\right)+mg=0 \tag{9}$$

for the y direction. Here, the drag force on the particle is balanced by its buoyant weight and particle-wall interactions have been ignored. (Note that gravity is arbitrarily defined to be in the positive y direction for the sake of discussion.) For convenience, the trajectory equations are cast in dimensionless form. The characteristic length is based on the wavenumber at the lower frequency,

$$x^* \equiv (2\kappa_1/\pi)x \tag{10a}$$

$$y^* \equiv (2\kappa_1/\pi)y \tag{10b}$$

while the characteristic time based on the flow speed to the right

$$t^* \equiv \frac{3\kappa_1^2 Q_1}{\pi^2}\,t \tag{11}$$

Thus, for the first step of the cycle, the dimensionless trajectory equations are

$$\frac{\partial x^*}{\partial t^*} = A\sin(\pi x^*) \tag{12a}$$

and

$$\frac{\partial y^*}{\partial t^*} = x^*(2-x^*)+B \tag{12b}$$

where the dimensionless group A is the ratio between the acoustic force and viscous drag due to the transverse fluid flow

$$A \equiv \frac{4\pi R^2 F E_{ac,1}}{9\mu Q_1}, \tag{13}$$

and B is the ratio between gravitational forces and viscous drag,

$$B \equiv \frac{4\pi R^2(\rho_p - \rho_f)g}{27\mu\kappa Q_1}. \tag{14}$$

In the second part of the cycle, we allow the higher-frequency sound field to have a different intensity than the low-frequency field. Also, the chamber may not be resonant at exactly double the frequency of the first step of the cycle. In this case, the trajectory equations are

$$\frac{\partial x^*}{\partial t^*} = \beta\Gamma A \sin(\Gamma\pi x^*) \tag{15a}$$

and

$$\frac{\partial y^*}{\partial t^*} = -\delta x^*(2 - x^*) + B. \tag{15b}$$

In Eq. 15, β is the ratio of the intensity of the acoustic field at the high frequency relative to that at the low frequency

$$\beta \equiv \frac{E_{ac,2}}{E_{ac,1}}, \tag{16}$$

and Γ is the ratio of the two frequencies used,

$$\Gamma \equiv \frac{f_2}{f_1} = \frac{\kappa_2}{\kappa_1} \tag{17}$$

which has a value close to 2.

The system of Eqs. 12 and 15 does not have a straightforward analytical solution so a numerical method was used to obtain model predictions. The simulation was performed by assigning the initial position of a large number of particles (N) to be distributed uniformly over x^* at $y^* = 0$. The net displacement of each particle, which depends on its starting position as well as the operating parameters for the cycle, was determined after the completion of one cycle. The arithmetic average displacement of the group of particles at the end of the two-step cycle was then calculated. Simulation of particle trajectories for more than one cycle involves repeated solution of Eqs. 12 and 15 using, as initial conditions, the final positions of the particles after completion of the previous step.

After simulating about five cycles, the limiting vertical positions of the trajectories are usually evident. Generally the simulations were carried out for a total of 30 cycles for accuracy. For a given set of acoustic and flow field parameters (α, β, B, κ_1, Q_1, t_1), a unique A (denoted as A_{cut}) can be identified for which the average displacement is zero. This critical value, which indicates the manner in which the suspension is fractionated, is found by a trial-and-error procedure. On the average, particles with $A > A_{cut}$ will move toward the right end of the chamber, and conversely the bulk of particles with $A < A_{cut}$ move leftward. The corresponding values for the critical particle size and/or acoustic contrast is then readily found from Eq. 13.

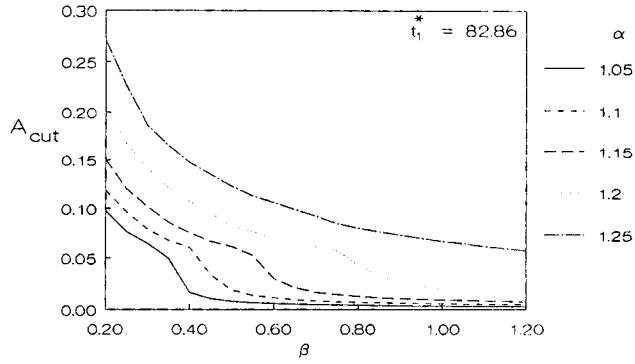

Figure 5. Sample model predictions for A_{cut} as a function of β and α for the example in the text.

Model Predictions

To demonstrate the potential and controllability of the fractionation method, sample model predictions are presented in this section. The case of negligible effect of gravity will be discussed first.

The model described above is applicable only when the assumptions that led to the trajectory equations are satisfied (see Appendix). Secondary acoustic forces can cause agglomeration and lower the sensitivity of the method to particle size. Higher frequency and energy density can be applied to increase the rate of particle response, but this must be limited to avoid the disruptive action of acoustic streaming and cavitation (Apfel, 1990; Gould et al., 1992). For these reasons, a useful operating range for frequency is 0.2–3 MHz and for energy density 0–100 J/m^3. The parameter β can vary in a wide range, but it will become evident that the most effective operation is achieved for $0.1 \le \beta \le 1.2$.

As an example, consider an aqueous suspension of polystyrene particles with $F = 0.23$, $R = 1 \times 10^{-6}$ m, $\rho_p - \rho_f = 50$ kg/m^3, $\mu = 10^{-3}$Pa·s, irradiated by 0.706 MHz, 10 J/m^3 ultrasound, with flow parameters $Q_1 = 7.36 \times 10^{-6}$ m^2/s and $t_1 = 4.13$ s. This system is characterized by $A = 4.2 \times 10^{-4}$ and $B = 1.03 \times 10^{-5}$. Since $B << A$, it is possible to neglect the effect of sedimentation of the particles on the calculated A_{cut}. Figure 5 shows the predicted A_{cut} as a function of β, for several values of the parameter α for this example. As α decreases, A_{cut} decreases indicating, among other things, that a smaller maximum particle size emerges in the product stream, but this is achieved at the expense of reduced production rate (cf. Eq. 7). As $\alpha \to 1$, $A_{cut} \to 0$ as expected since this approaches the batch mode of operation in which the left end of the acoustic chamber is depleted from all particle types. Also, as β increases, A_{cut} decreases because all particles response faster to higher energy density acoustic fields in the second part of each cycle. From Figure 5, it is apparent that A_{cut} is most sensitive to β in the range $0.1 \le \beta \le 1.2$.

As the particle size and/or the density difference between the particles and the medium increase, sedimentation assists the motion of the particles to the right and resists the motion to the left. Figure 6 shows the effect of sedimentation on the particle cut size for polystyrene particles under typical exper-

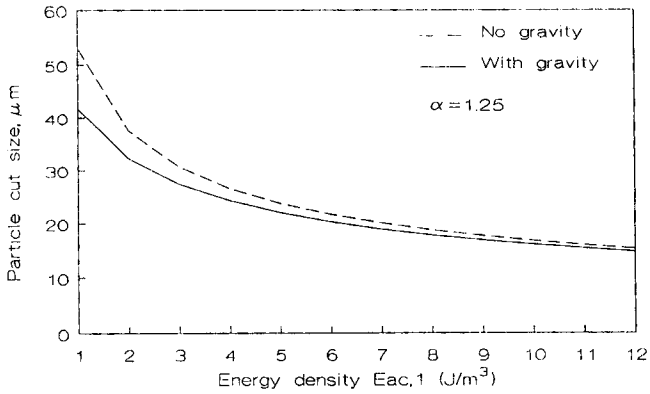

Figure 6. Sample model predictions for the cut particle size as a function of energy density and α for the example in the text.

Also indicated is the effect of sedimentation on the fractionation.

imental conditions: $t_1 = 4.13$ s, $\alpha = 1.25$, and $\beta = 0.51$. The particle cut size decreases with increasing acoustic energy density $E_{ac,1}$. The effect of sedimentation is more profound at low energy densities, where the particle cut size is large.

Experimental Procedure

Proof-of-principle experiments were performed in the acoustic chamber, as shown in Figure 7. A rectangular lead zirconate titanate transducer (APC 880, 38.1 × 25.4 × 2.03 mm) supplied by APC Company was supported on a rubber gasket (Neoprene 0.81 mm) in an aluminum frame. A rectangular glass reflector (38.1 × 25.4 × 0.9 mm) was similarly placed in another aluminum frame. A teflon sheet (1.01 mm) with its central section removed acted as a spacer. The whole assembly was clamped together to define a rectangular channel (38.1 × 19 × 1.08 mm). The chamber was oriented so that gravity was parallel to the direction of flow. At the two ends of the channel, ports allowed feed introduction and product removal with the help of a computerized peristaltic pump (Masterflex 7550-90). The electrical excitation for the transducer was generated by a Krohn-Hite 2100A Generator and amplified by an ENI 240L Power Amplifier. The electrical energy input was measured by a Bird 4410A Wattmeter. The coordination between the pump and signal generator was provided by an AT-type computer.

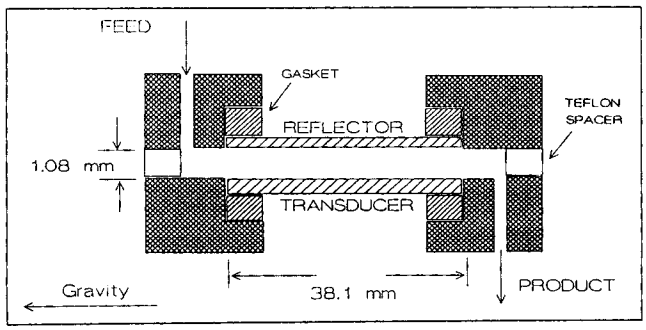

Figure 7. Fractionation chamber used in the experiments.

The two-step cycle described previously was applied. Feed was introduced at the bottom of the acoustic chamber and the product stream was withdrawn from the top. Particles smaller than the cut size, emerging at the product stream, were collected and analyzed. Particles larger than the cut size migrate to the bottom of the acoustic chamber where they concentrate. These particles are removed at the end of the experimental run. Truly continuous operation would be achieved if a purge stream was used to remove particles from the bottom of the chamber keeping their concentration constant. However, the experimental procedure followed closely resembles continuous operation for low feed concentrations and short operation times.

Another acoustic cell similar to the one described previously was constructed to enable visualization of the particle collection during the low- and high-frequency steps. The reflector was attached on a micrometer-controlled stage so that precise positioning (±5 μm) was achieved. The side walls were made of Plexiglass so direct observation through the chamber was possible. The first of the photographs in Figure 8 shows a uniform suspension of 325-mesh polystyrene particles between the transducer and the reflector. The second photograph demonstrates collection of the particles to the center of the acoustic chamber after irradiation with 0.732 MHz, 20 J/m^3 sound. The third photograph illustrates collection of particles midway between the center and the walls of the acoustic chamber, after irradiation with 1.435 MHz, 20 J/m^3 sound. Note the distinct layers into which the particles are collected.

To compare model predictions to the experimental results, the value of E_{ac} is needed. However, due to the effects of resonance, diffraction and losses, the relation between the measured electric energy input and E_{ac} is not straightforward. The small dimensions of the acoustic cell and the high frequencies used do not allow direct measurement of the excess acoustic pressure with a hydrophone. Instead, a method developed in our laboratories was used (Mandralis, 1993). According to this method, a micron-sized sphere is suspended in the standing wave field, and its equilibrium position is precisely determined using a microscope. By balancing the acoustic force predicted by Eq. A1 (see Appendix) with the buoyant weight of the particle, the acoustic energy density can be determined to within ±20% (Mandralis, 1993).

The particle-size distribution and particle number density of the product stream were determined by placing a small sample of the stream between two microscope slides that were spaced 0.076 mm apart. A CUE-2 Image Analysis software installed on an AT computer and an optical microscope was used to analyze the particle-size distribution. For each measurement, a large number of particles were analyzed to get statistically meaningful results. The same procedure was followed for determining the characteristics of the feed stream. Using this method, only particles larger than about 2 μm could be accurately identified and counted.

Comparison of Theory and Experiments

Several experiments were performed to demonstrate the effectiveness of the fractionation technique and obtain data to complement the theoretical development. The resonant frequencies for the acoustic chamber were experimentally determined to be 0.706 MHz and 1.435 MHz which provided rapid collection of particles at the nodes of each part of the cycle.

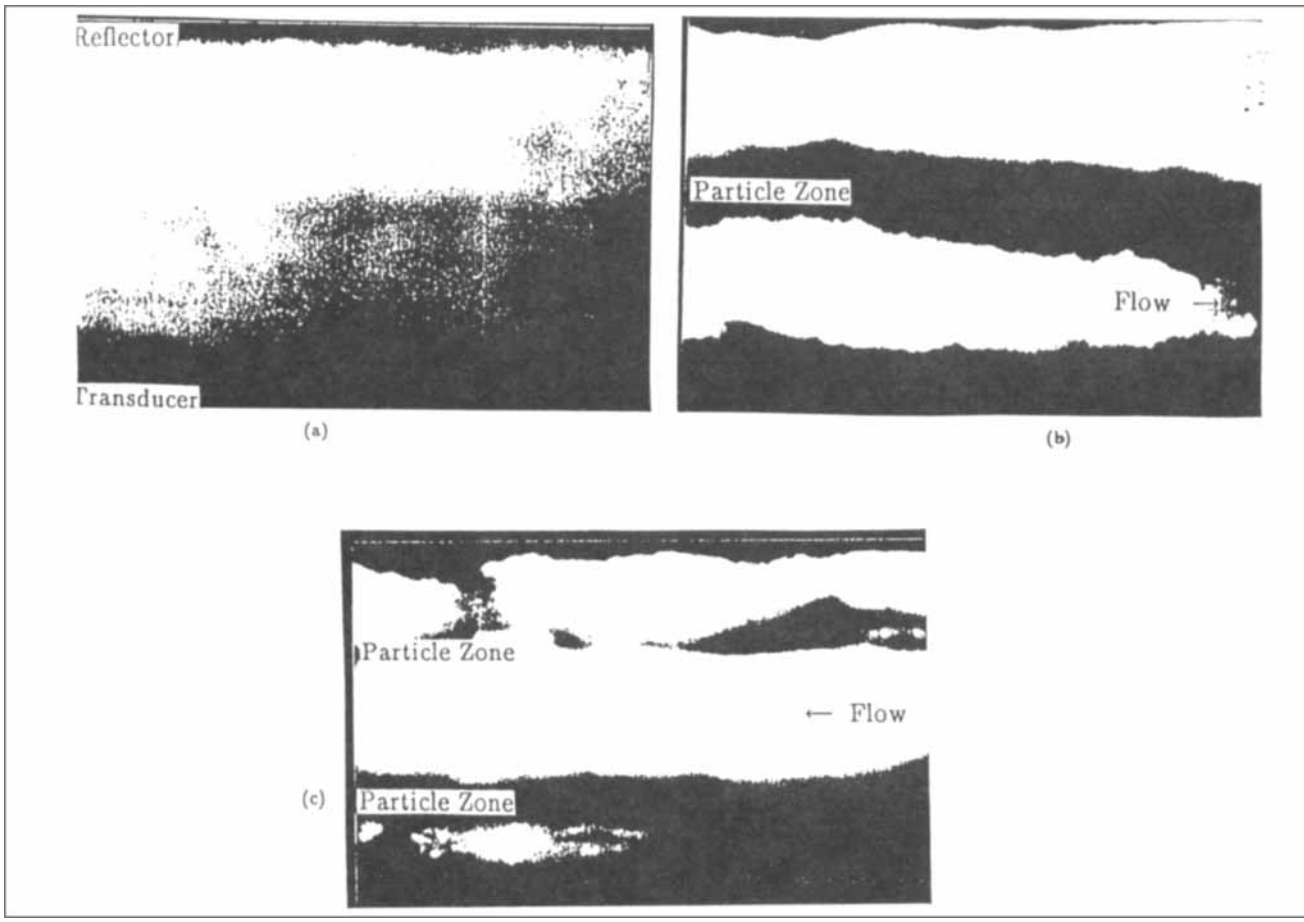

Figure 8. Acoustic response of the 325-mesh polystyrene particles.

Each photograph is a side view of the gap between the transducer (bottom wall of the gap) and the reflector (top wall of the gap): (a) suspension before the application of ultrasound—particles are uniformly distributed; (b) suspension subjected to the low-frequency acoustic field—particles collect at the midplane of the chamber; (c) suspension subjected to the high-frequency acoustic field—particles collect in planes located at 1/4 of the gap width from the walls.

Depending on the force applied during clamping of the chamber, the resonant frequencies were reproducible to within 2%. The flow rate was fixed at $Q_1 = Q_2 = 7.36 \times 10^{-6}$ m^2/s for all experiments. Suspensions of 325-mesh polystyrene particles in distilled water, which contained about 0.01% w/w sodium dodecyl sulfate (SDC) to prevent particle agglomeration, were fed to the chamber.

The first set of experiments was performed at $\alpha = 1.25$ ($t_1 = 4.13$ s, $t_2 = 5.16$ s) which resulted in $Q_{prod} = 0.81 \times 10^{-6}$ m^2/s. The particle concentration was about 1% w/w, and the electric energy input varied in the range 0.2–1.7 W. To compare the experimental results with the theoretical predictions, the method described in the previous section was used to determine the acoustic energy density from the measured electric energy input. The acoustic energy densities were chosen such that $\beta \approx 0.51$ for this set.

Table 1 shows the particle number density, mean radius and standard deviation for the feed and product streams at steady state for various acoustic energy densities. The number of particles in the product stream as well as the mean particle radius and standard deviation decrease as the acoustic energy density increases, in agreement with theoretical expectations. A more detailed picture of the effect of the energy density on the particle cut size is given in Figure 9 which shows the particle-size distribution of the feed and the product stream for the same experimental conditions used in Table 1. The vertical dashed line is the theoretical particle cut size obtained directly from the model predictions.

Figure 9 shows that, in accordance with the theory, very few particles larger than the cut size emerge at the product stream. However, the experimentally achieved fractionation was not as sharp as the theoretical prediction. Many of the smaller particles that should have emerged in the product stream did not. This is attributed to secondary acoustic forces which probably resulted in agglomeration of the smaller particles; these agglomerates behave as larger particles giving them an effective

Table 1. Particle Statistics for Product Stream for Various Values of $E_{ac,1}$ at $\alpha = 1.25$*

$E_{ac,1}$ (J/m^3)	β	No. Density (Particles/cm^3)	Mean Radius (μm)	Std. Dev. (μm)
0	—	1,469,816	9.61	5.50
3.3	0.51	770,341	5.57	3.40
3.8	0.51	557,742	5.52	3.39
6.5	0.51	353,018	4.33	2.40
11.1	0.51	65,676	4.88	2.72

*The table entry for $E_{ac,1} = 0$ indicates the statistics for the feed to the chamber.

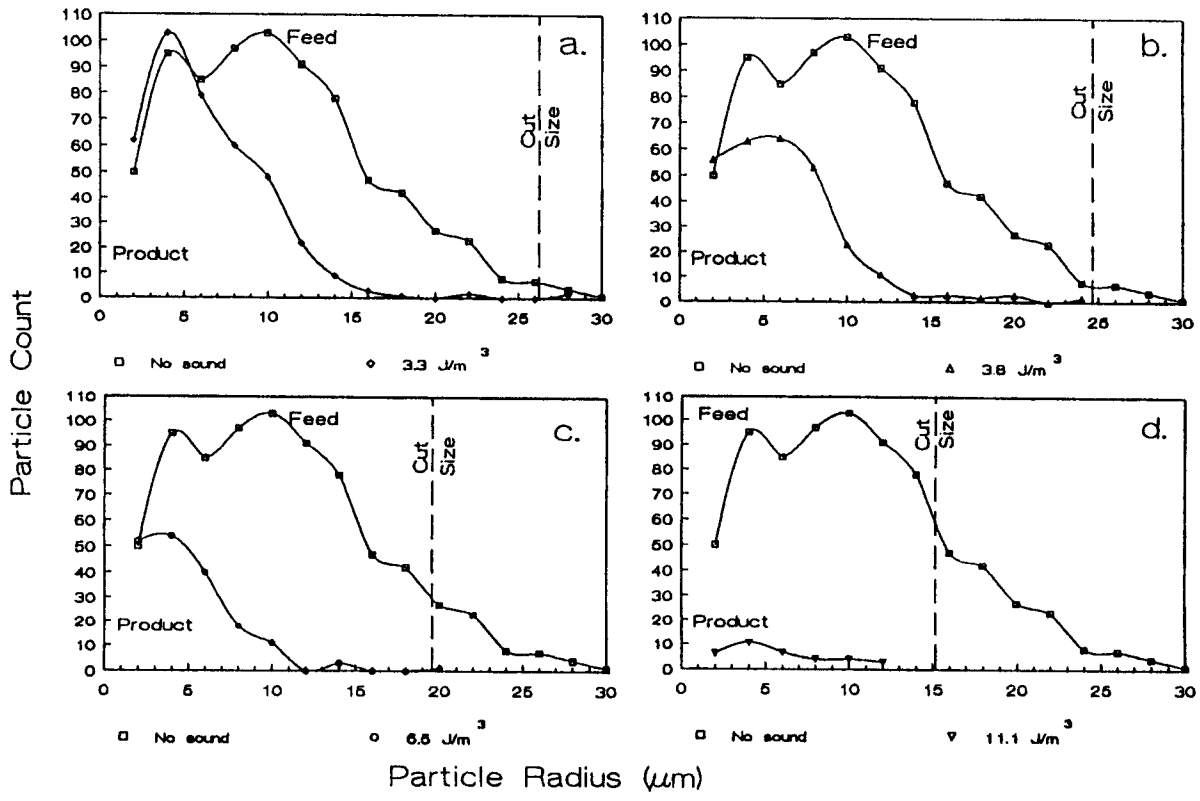

Figure 9. Product stream particle-size distributions obtained for several values of $E_{ac,1}$ with $\alpha = 1.25$ and $\beta = 0.51$.

Also shown in each graph are the particle-size distributions for the polystyrene suspension fed to the chamber. The vertical dashed lines represent the theoretical cut particle size predicted from the model.

A larger than A_{cut} and resulting in their exclusion from the product stream.

Another set of experiments was conducted at $\alpha = 1.15$ ($t_1 = 4.13$ s, $t_2 = 4.76$ s) which results in $Q_{prod} = 0.15 \times 10^{-6}$ m^2/s. The particle concentration was about 2% w/w. Electrical power input in the range 0.2–1.7 W was used to give a series of β values ranging from 0.57 to 0.75. Table 2 shows the particle statistics for the feed and the product stream for various energy levels. In agreement with theoretical predictions, fewer and smaller particles energy at the product stream with increasing the sound field intensity. Figure 10 shows the particle-size distribution for the same set of experiments. Again, the dashed lines denote the theoretical values obtained for the particle cut size. The agreement between observed and calculated particle cut size is good for the lower acoustic energy density used. The effect of particle agglomeration is again evident. As the sound intensity increases, the particle cut size drops below 5 μm, but there are some particles in the range 5–10 μm that emerge at the product stream. This can be explained by the fact that smaller particles are only slightly affected by the combined effects of the alternating sound field and the bidirectional flow field. Thus, small flow disturbances due to wall and edge effects or deviations from the uniform, planar standing wave field configuration might change the final destination of smaller particles.

Conclusions

A fractionation method for fine particles in liquid suspensions has been developed. The method is based on the transient response of the particles to alternating low- and high-frequency ultrasonic standing wave fields. Fast and controllable partial separations across the thin dimension of a rectangular channel can be achieved. Transverse, bidirectional, laminar flows amplify these partial separations into useful separations along the channel. Continuous fractionation of micron-sized particles based on size differences has been demonstrated experimentally. Fractionation of materials with different density and/or compressibility is also possible, and experiments will continue in this direction. The particle cut size can be continuously adjusted by changing the sound frequency and intensity or the flow rate.

Although sharp fractionation of the polystyrene suspensions was achieved, the yield was below theoretical predictions due to agglomeration of smaller particles resulting from secondary acoustic forces. Even though the magnitude of the secondary

Table 2. Particle Statistics for Product Stream for Various Values of $E_{ac,1}$ at $\alpha = 1.25$*

$E_{ac,1}$ (J/m^3)	β	No. Density (Particles/cm^3)	Mean Radius (μm)	Std. Dev. (μm)
0	—	2,690,288	9.87	5.88
3.3	0.57	892,398	3.95	1.88
4.7	0.59	692,913	3.77	1.85
6.6	0.68	423,884	3.64	1.87
11.3	0.74	368,766	3.26	1.33

*The table entry for $E_{ac,1} = 0$ indicates the statistics for the feed to the chamber.

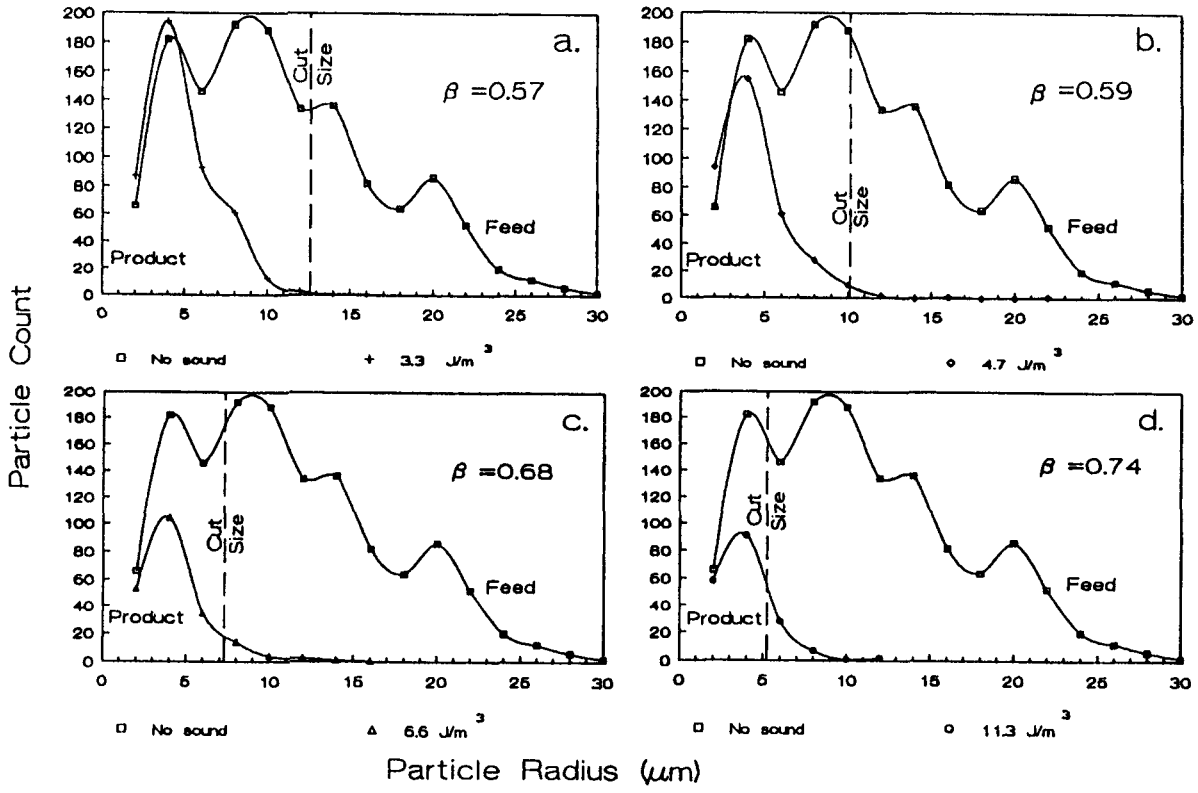

Figure 10. Same as Figure 9, but with $\alpha = 1.15$ and β ranging from 0.57 to 0.74.

forces is several orders smaller than the magnitude of the primary acoustic force, their effect on the motion of the particles can be significant due to the long residence time of the particles in the acoustic chamber ($\approx$ 1 min). More susceptible to agglomeration are the larger, denser and less compressible particles in concentrated suspensions. If removal of all particles from the product stream is desired, then agglomeration might be helpful and should be promoted.

Contamination of the product stream with particles larger than the cut size occurred, especially at smaller cut sizes. Multiple-stage operation should alleviate this problem. The effective number of separation stages within a single chamber can be increased (at the expense of production rate) without hardware changes by simply reducing the stroke size ($Q_1 t_1$).

The experimental work reported here was based on a single channel device. For larger production rates, several transducers combined in a mosaic structure can be used. In addition, the distance between the transducer and the reflector can be several wavelengths. Thin or acoustically transparent layers can subdivide the chamber into many parallel channels serviced by a single generator, amplifier, and pumping mechanism.

Acknowledgment

Nestlé has provided partial support for this research through a Westreco Fellowship.

Notation

b = channel half-height, m
c = speed of sound, m/s
d = center to center interparticle distance, m
E_{ac} = time averaged acoustic energy density, J/m^3
f = frequency, s^{-1}
F = acoustic contrast Eq. A2, dimensionless
g = gravity acceleration, 9.81 m/s^2
m = $4/3\pi\,(\rho_p - \rho_f)R^3$, buoyant particle mass, kg
n = particle number density, m^{-3}
N = total number of particles
P_{ac} = pressure amplitude of incident acoustic wave, Pa
Q = flow rate per unit width, m^2/s
R = particle radius, m
t = time, s
u_f = local flow velocity, m/s
U_{ac} = velocity amplitude of incident acoustic wave, m/s
V = particle volume, m^3
x = particle position across the channel relative to the transducer, m
y = particle position along the channel, m

Greek letters

α = $Q_2 t_2 / Q_1 t_1$, relative stroke volumes, dimensionless
β = $E_{ac,2}/E_{ac,1}$, relative acoustic energy densities, dimensionless
γ = $1/\rho c^2$, compressibility m^2/N
δ = Q_2/Q_1
Γ = f_2/f_1, relative frequencies, dimensionless
κ = $2\pi/\lambda$ wave number, m^{-1}
λ = c/f = wavelength of sound, m
μ = viscosity, Pa·s
ρ = density, kg/m^3
ω = angular frequency, rad/s

Subscripts and superscripts

$_{cut}$ = cut (critical) particle type
$_f$ = fluid
$_i$ = ith particle
$_{if}$ = infinitely fast particle
$_p$ = particle
$_{prod}$ = product stream

$_{zc}$ = zero-contrast particle
$_0$ = initial value
$_1$ = step 1
$_2$ = step 2
* = dimensionless variable

Literature Cited

Apfel, R. E., "Radiation Pressure—Principles and Application to Separation Science," Fortschritte der Acustik DAGA, 19, Wien (1990).

Apfel, R. E., "Acoustically Induced Square Law Forces and Some Speculations about Gravitation," *Am. J. Phys.*, **56**, 726 (1988).

Collas, P., M. Barmatz, and C. Shipley, "Acoustic Levitation in the Presence of Gravity," *J. Acoust. Soc. Amer.*, **86**, 777 (1989).

Gould, R. K., W. T. Coakley, and M. A. Grundy, "Upper Sound Pressure Limits on Particle Concentration in Fields of Ultrasonic Standing—Wave at Megahertz Frequencies," *Ultrasonics*, **30**, 239 (1992).

Haar, G., and S. J. Wyard, "Blood Cell Banding in Ultrasonic Standing Wave Fields: a Physical Analysis," *Ultrasound in Med. & Biol.*, **4**, 111 (1978).

Hager, F., E. Benes, W. Bolek, and M. Gröschl, "Investigation of a New Ultrasonic Drifting Resonance Field Cell for the Refinement of Aerosols," *Proc. FASE Symp.*, 261, Hungary (1991).

Higashitani, K., M. Fukushima, and Y. Matsuno, "Migration of Suspended Particles in Plane Stationary Ultrasonic Field," *Chem. Eng. Sci.*, **36**, 1877 (1981).

King, L. V., "On the Acoustic Radiation Pressures on Spheres," *Proc. Roy. Soc. London*, **147A**, 212 (1934).

Mandralis, Z. I., D. L. Feke, and R. J. Adler, "Transient Response of Fine-Particle Suspensions to Mild Planar Ultrasonic Fields," *Fluid/Particle Sep. J.*, **3**, 115 (1990).

Mandralis, Z. I., and D. L. Feke, "Continuous Suspension Fractionation Using Acoustics and Divided Flow Fields," *Chem. Eng. Sci.*, in press (1993).

Mandralis, Z. I., "Fractionation of Fine-Particle Suspensions by Combined Ultrasonic and Flow Fields," PhD Diss., Case Western Reserve Univ., Cleveland, OH (1993).

Peterson, S. C., U.S. Patent No. 4,759,775 (1988).

Schram, C. J., U.S. Patent No. 4,743,361 (1988).

Schram, C. J., and M. Rendell, "Manipulation of Particles in Megahertz Standing Waves," *Proc. Ultrasonics Int. Conf.*, 262 (1989).

Tolt, T. L., and D. L. Feke, "Analysis and Application of Acoustics to Suspension Processing," *ASME Intersociety Energy Conversion Engineering Conf.*, **4**, 327 (1988).

Tolt, T. L., and D. L. Feke, "Separation of Dispersed Phases from Liquids in Acoustically Driven Chambers," *Chem. Eng. Sci.*, **48**, 527 (1993).

Weiser, M. H., R. E. Apfel, and E. A. Neppiras, "Interparticle Forces on Red Cells in a Standing Wave Field," *Acustica*, **56**, 114 (1984).

Whitworth, G., M. A. Grundy, and W. T. Coakley, "Transport and Harvesting of Suspended Particles Using Modulated Ultrasound," *Ultrasonics*, **29**, 439 (1991).

Yosioka, K., and Y. Kawasima, "Acoustic Radiation Pressure on a Compressible Sphere," *Acustica*, **5**, 167 (1955).

Appendix

The principal acoustic force acting on an individual spherical particle with radius much smaller than the wavelength of sound, suspended in a standing wave field created by oppositely traveling, single-frequency, sinusoidal sound waves was first analyzed by King (1934) for the case of a rigid particle. Kawasima and Yosioka (1955) extended the analysis to include the case of compressible spheres. Their result for the time-averaged acoustic radiation force, F_{ac}, is given by:

$$F_{ac} = 4\pi R^3 \kappa E_{ac} F \sin(2\kappa x). \tag{A1}$$

The acoustic contrast factor F accounts for the material properties of the suspension and is given by:

$$F = \frac{1}{3}\left[\frac{5\rho_p - 2\rho_f}{\rho_f + 2\rho_p} - \frac{\gamma_p}{\gamma_f}\right] \tag{A2}$$

If $F>0$, the particles are urged toward the pressure nodes; conversely, if $F<0$, the particles are collected at the pressure antinodes.

When two particles suspended in an acoustic field are close to each other, a secondary acoustic field, first described by Bjerknes, arises due to the acoustic field emitted from each particle to other particles in its vicinity. This force is attractive when both particles are either more or less compressible than the fluid and repulsive in any other case. For the general case of two particles of different volumes and compressibilities, the Bjerknes force is given by (see Apfel, 1988):

$$F_b = \frac{\rho_f}{8\pi}(\omega P_{ac})^2 \gamma_f^2 \left(1 - \frac{\gamma_{p1}}{\gamma_f}\right)\left(1 - \frac{\gamma_{p2}}{\gamma_f}\right)\frac{V_1 V_2}{d^2} \tag{A3}$$

For two rigid spheres oscillating due to an acoustic wave field that propagates perpendicular to their line of centers, an attraction force arises given by (Weiser, 1984):

$$F_h = \frac{\pi(\rho_p - \rho_f)^2 U_{ac}^2 R^6}{3\rho d^4} \tag{A4}$$

Lateral primary forces might also arise due to diffraction effects, edge effects, and/or nonuniform performance of the acoustic transducer. For the experimental conditions of this work, observation of the particle trajectories showed that these lateral forces are about two orders of magnitude smaller than the primary acoustic force.

A typical system consists of polystyrene particles $R = 1 \times 10^{-6}$ m, $F = 0.22$, suspended in a standing wave field of $f = 1 \times 10^{-6}$ Hz, $E_{ac} = 10$ J/m^3. The interparticle center-to-center distance for a highly concentrated system could be in the order of $d = 3 \times 10^{-6}$ m. For this system, Eq. A1-A4 give the magnitude of the various forces:

$$F_{ac} = 0.13 \times 10^{-12}\text{N},\ F_h = 0.14 \times 10^{-14}\text{N},\ F_b = 0.19 \times 10^{-16}\text{N}$$

It is obvious that both attraction forces are at least two orders of magnitude smaller than the primary acoustic force and therefore do not affect the particle trajectories for short irradiation times.

Manuscript received Aug. 28, 1992, and revision received Nov. 20, 1992.